AGU PUBLICATIONS

JGR

Journal of Geophysical Research: Oceans

RESEARCH ARTICLE

10.1002/2015JC011180

Special Section:
Forum for Arctic Modeling and Observing Synthesis (FAMOS): Results and Synthesis of Coordinated Experiments

On the vertical phytoplankton response to an ice-free Arctic Ocean

J. Lawrence[1,2], E. Popova[1], A. Yool[1], and M. Srokosz[1]

[1]National Oceanography Centre, Southampton, UK, [2]National Oceanography Centre, University of Southampton, Southampton, UK

Abstract Rapidly retreating sea ice is expected to influence future phytoplankton production in the Arctic Ocean by perturbing nutrient and light fields, but poor understanding of present phytoplankton distributions and governing mechanisms make projected changes highly uncertain. Here we use a simulation that reproduces observed seasonal phytoplankton chlorophyll distributions and annual nitrate to hypothesize that surface nitrate limitation in the Arctic Ocean deepens vertical production distributions where light-dependent growth rates are lower. We extend this to interpret depth-integrated production changes projected by the simulation for an ice-free Arctic Ocean. Future spatial changes correspond to patterns of reduced surface nitrate and increased light. Surface nitrate inventory reductions in the Beaufort Gyre and Atlantic inflow waters drive colocated production distributions deeper to where light is lower, offsetting increases in light over the water column due to reduced ice cover and thickness. Modest production increases arise, 10% in a seasonally ice-free Arctic Ocean and increasing to 30% by the end of the century, occurring at depth.

Key Points:
- We use a 1/4° ocean biogeochemical model to assess Arctic primary production
- Net primary production is linked to nitrate-light conditions
- Application to future production suggests modest increases, occurring at depth

Supporting Information:
- Supporting Information S1

Correspondence to:
J. Lawrence,
jonathan.lawrence@noc.soton.ac.uk

Citation:
Lawrence, J., E. Popova, A. Yool, and M. Srokosz (2015), On the vertical phytoplankton response to an ice-free Arctic Ocean, *J. Geophys. Res. Oceans*, *120*, doi:10.1002/2015JC011180.

Received 31 JUL 2015
Accepted 3 DEC 2015
Accepted article online 9 DEC 2015

1. Introduction

Rapid reductions in Arctic sea ice thickness [*Laxon et al*., 2013] and extent [*Serreze et al*., 2007; *Stroeve et al*., 2012], increased seasonality [*Serreze et al*., 2007] and shifts from perennial to first year ice [*Stroeve et al*., 2012], are underway. Reductions in sea ice and changes in seasonality are expected to modify stratification and momentum transfer to the ocean (for example, through internal wave generation [*Rainville and Woodgate*, 2009] and changes in ocean wind stress [*Carmack and Chapman*, 2003; *Davis et al*., 2014]), which modulates nitrate supply to the euphotic zone [*Popova et al*., 2006]. Reductions in ice thickness and extent will also impact light available for photosynthesis [*Arrigo et al*., 2008; *Arrigo and van Dijken*, 2015].

Changes are already underway in the Canada Basin [*McLaughlin et al*., 2011]. Freshwater accumulation [*Giles et al*., 2012], probably arising from increased momentum transfer to the ocean [*Giles et al*., 2012; *Davis et al*., 2014], has driven a general increase in stratification [*McLaughlin et al*., 2011]. Convergence and stratification increases have driven concomitant reductions in surface nitrate [*McLaughlin and Carmack*, 2010], deepening summer chlorophyll maxima [*McLaughlin and Carmack*, 2010; *Bergeron and Tremblay*, 2014], and favoring phytoplankton with smaller cell sizes that are more efficient at nutrient uptake [*Li et al*., 2009]. These changes are likely due to a combination of both long-term sea ice retreat and decadal changes in the wind-driven circulation [*Proshutinsky et al*., 2002]. For example, freshening of the surface Arctic Ocean arising from climatic changes in precipitation [*Bintanja and Selten*, 2014], runoff, and sea ice cover [*Peterson et al*., 2006] is exacerbated by increased freshwater storage in the Canadian Arctic Ocean under current decadal wind patterns [*McLaughlin et al*., 2011; *Giles et al*., 2012].

Phytoplankton distributions and growth are expected to continue to respond to sea ice retreat but controlling mechanisms across the Arctic Ocean remain unclear [*Arrigo et al*., 2008; *Tremblay and Gagnon*, 2009; *Codispoti et al*., 2013; *Brown et al*., 2015]. Consequently, even the direction of future changes in Arctic Ocean production is highly uncertain [*Steinacher et al*., 2010; *Popova et al*., 2012; *Vancoppenolle et al*., 2013].

In particular, substantial phytoplankton growth can occur under ice [*Arrigo et al*., 2012; *Matrai and Apollonio*, 2013] and in photosynthetically competent subsurface chlorophyll maxima [*Hill and Cota*, 2005; *McLaughlin and Carmack*, 2010], but the distribution and magnitude of under ice and subsurface production remain

unclear [*Arrigo et al*., 2011; *Hill et al*., 2013; *Martin et al*., 2013] because they are not retrievable by satellite [*Smith*, 1980; *Pabi et al*., 2008].

Here we use a simulation that reproduces observed phytoplankton chlorophyll distributions across the Arctic Ocean, including in subsurface chlorophyll maxima and under ice, to elucidate what governs vertical net production distributions over the seasonal cycle. We will then use this generalizable response of Arctic Ocean phytoplankton to nitrate and light conditions to explain simulation-projected changes in depth-integrated net production (hereafter production) in terms of its vertical distribution.

2. Methods

2.1. Simulation Description

For the simulation, an intermediate complexity biogeochemical model (MEDUSA) [*Yool et al*., 2013], embedded within a general circulation model (NEMO) that comprises ocean (OPA) [*Madec*, 2008] and ice (LIM2) [*Timmermann et al*., 2005] components, is run to 2099 at a global-average model resolution of 1/4°. The grid is nonlinear and resolution increases toward the poles. For example, resolution at 60°N is ~16.8 km. The model is forced with output from HadGEM-ES [*Collins et al*., 2011] under representative concentration pathway (RCP) 8.5 [*Riahi et al*., 2011]. Production is calculated for two phytoplankton classes. This is done by modulating a temperature-dependent theoretical maximum production rate, as per *Eppley* [1972], by standard Michaelis-Menten nutrient limitation and hyperbolic light limitation terms. Photoacclimation is factored in through a chlorophyll-specific initial slope of the photosynthesis-irradiance curve. Full details can be found in *Yool et al*. [2013].

2.2. Defining Production, Nitrate, and Light Metrics

Here we consider pan-Arctic Ocean net primary production (hereafter primary production or production): the biological uptake of inorganic nutrients from physical supply in waters north of 65°N. To describe the vertical structure of primary production across the Arctic Ocean, we consider production that occurs above and below a reference depth. Throughout the analysis, we term the former as surface production (P_1) and the latter as subsurface production (P_2). Based on production distributions inferred from nitrate uptake [*Codispoti et al*., 2013; *Matrai and Apollonio*, 2013] and chlorophyll and production profiles [*Martin et al*., 2010; *McLaughlin and Carmack*, 2010; *Brown et al*., 2015], we chose a reference depth of 20 m (explained in section 4). The subsurface fraction of production is defined as that which occurs below the reference depth

$$\mathrm{Prop} = \frac{P_2}{P_1 + P_2}, \tag{1}$$

giving a simple metric that can be related to ambient nitrate and light conditions. Nitrate is dominantly supplied to the euphotic zone through winter mixing [*Tremblay and Gagnon*, 2009; *Popova et al*., 2010; *Codispoti et al*., 2013; *Randelhoff et al*., 2015] and taken up by phytoplankton in summer [*Arrigo et al*., 2008]. We therefore define an annual nitrate inventory (N_{inv}) as the nitrate concentration at the time of maximum mixed layer depth, integrated from the surface to the reference depth. Following previous observational studies [*Codispoti et al*., 2013; *Hill et al*., 2013; *Matrai et al*., 2013; *Randelhoff et al*., 2015], we take the main phytoplankton growth season in the Arctic Ocean to occur between July and September. We then define a solar radiation dose (SRD) as photosynthetically active (400–700 nm) radiation penetrating surface waters through sea ice cover, averaged over July–September and integrated to the reference depth. We use a static reference depth rather than mixed-layer depth, because observations [*Martin et al*., 2010; *McLaughlin and Carmack*, 2010] and our simulation (Figure 1) demonstrate that phytoplankton growth can occur below the mixed layer in summer.

At lower Arctic latitudes (toward 65°N), the phytoplankton growth season may start earlier than July. To test the validity of the July–September interval, we ran an additional analysis covering May–September. This analysis (see supporting information Figure S1) showed that the ability to predict vertical distributions of production declines when the interval is extended to include May and June, justifying the selection of July–September.

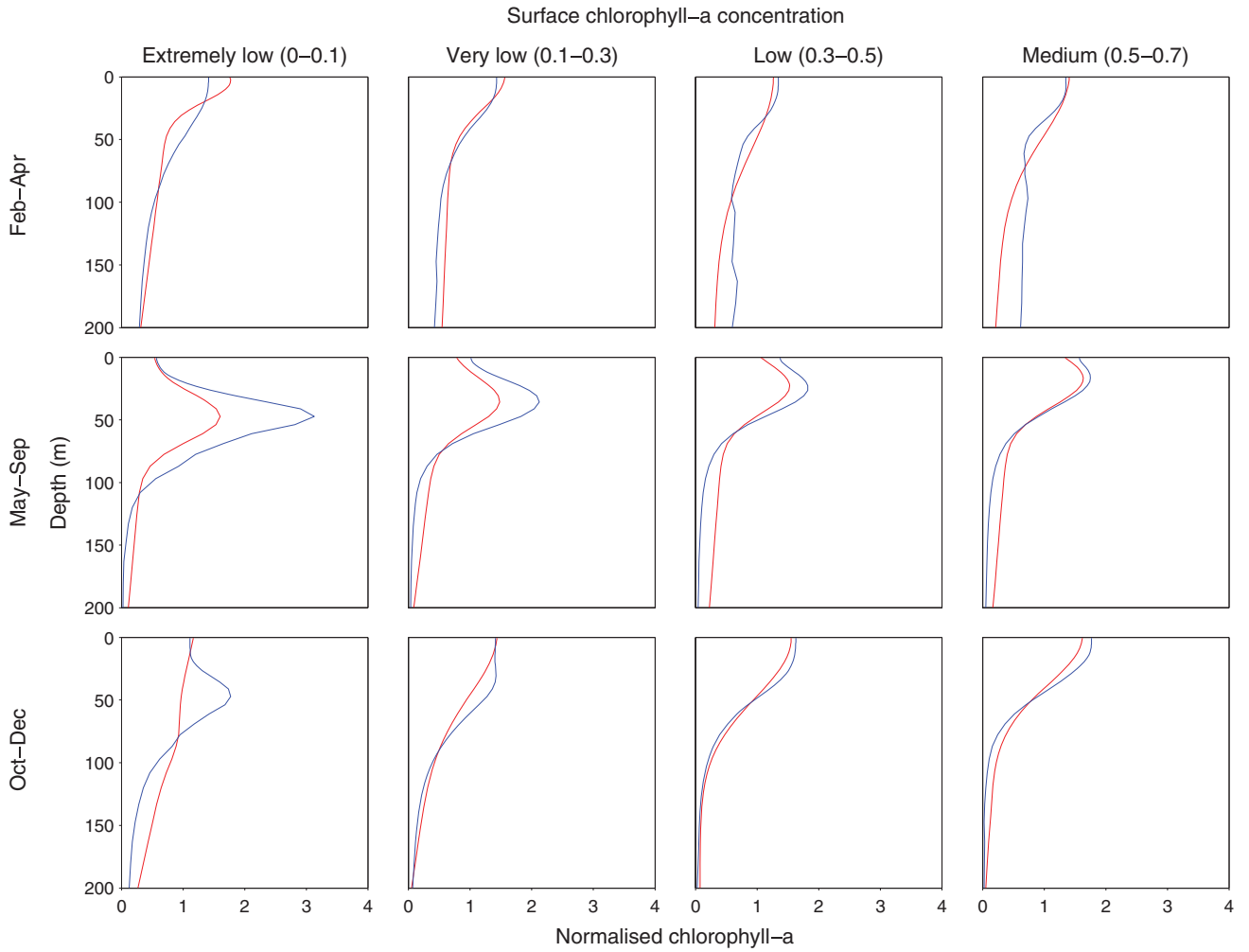

Figure 1. Observed (red) and simulated (blue) Arctic normalized chlorophyll-a profiles, sorted by season and surface chlorophyll concentration. Observations (n = 2403 profiles) span 1954–2007, whereas simulated profiles span 1990–2009. Locations where water depths are <50 m are omitted. Observations cover variable ice conditions but are biased toward open water and summer months; details of the observations can be found in *Ardyna et al.* [2014].

Deepening of production distributions in the projection is presented in terms of deepening chlorophyll and production maxima, where maxima are defined as the depth at which production and chlorophyll profiles are at their water column maximum value.

Surface nitrate depletion is masked at an inventory of 50 mmol m^{-2} to emphasize the spatial correspondence between low surface nitrate waters and production changes—the correspondence arises below this threshold because of the nonlinear dependence of nitrate limitation on ambient nitrate concentrations [*Monod*, 1949].

2.3. Building the Regression Model

We suggest that the vertical structure of Arctic Ocean primary production depends on N_{inv} and SRD. To demonstrate this, we determine how well a multilinear regression model based on the predictors N_{inv} and SRD can predict the spatial map of Prop (equation (1)) that arises from the full simulation. Because our simulation reproduces observed vertical distributions of phytoplankton (Figure 1), a regression model that can accurately predict Prop that arises in the full simulation implies that other variables, such as temperature, are not important in determining vertical production distributions across the Arctic Ocean. The ability of N_{inv} and SRD to predict the vertical distribution of production is tested by building a regression model that is then plotted against the full numerical simulation Prop. Thus, in this analysis, locations where the regression model reproduces the full simulation lie on a 1–1 line. Larger deviations from this line reflect

decreasing ability of the linear regression model to reproduce vertical production distributions in the full simulation, possibly either due to nonlinearities in the dependence of production on nitrate and light [*Bergeron and Tremblay*, 2014] or the importance of other variables in setting Prop.

2.4. Direct Temperature Impact on Production

The importance of surface-ocean warming on projected changes in depth-integrated production is testable in the simulation from the temperature dependence of phytoplankton growth rates [*Eppley*, 1972]. The simulated maximum growth rate of phytoplankton is directly dependent on temperature as

$$J_{max} = V_p * 1.066^T, \quad (2)$$

where V_p is the maximum growth rate at 0°C [*Eppley*, 1972; *Yool et al*., 2013]. This maximum growth rate is modulated by nitrate and light limitation such that it is only realized in nitrate and light replete conditions.

3. Results

3.1. Simulation-Observation Chlorophyll Comparison

The simulation reproduces observed Arctic Ocean seasonal chlorophyll distributions (Figure 1). Seasonal increases in light stimulate a spring bloom in nitrate replete surface waters with chlorophyll profiles decreasing with depth according to attenuation of light in the water column (top row). In more oligotrophic waters, surface nitrate depletion by the spring bloom promotes the subsequent development of a shade flora. The subsurface chlorophyll maxima that develop are more pronounced and occur deeper in more oligotrophic waters, a feature captured by the simulation (middle row). In autumn, increased mixing replenishes surface nitrate, and chlorophyll maxima return to surface waters (bottom row), accompanied in ice-free waters by a second bloom [*Ardyna et al*., 2014]. Deviation of the simulation from observed chlorophyll profiles is restricted to areas with extremely low surface chlorophyll where the model overestimates the strength of summer subsurface chlorophyll maxima and insufficiently homogenizes the vertical chlorophyll distribution during winter mixing (middle left and bottom left plots, respectively).

3.2. Simulation-Observation Nitrate Comparison

Nitrate is depleted in Arctic Ocean summer surface waters [*Codispoti et al*., 2013], limiting net community production across the Arctic Ocean [*Tremblay et al*., 2008; *Tremblay and Gagnon*, 2009; *Randelhoff et al*., 2015]. Here we compare simulated annual-average nitrate to the World Ocean Atlas 2013 (WOA) [*Garcia et al*., 2014] along a Pacific-Atlantic transect that traverses the Central Basin (Figure 2). Surface nitrate is broadly higher at lower latitudes (toward 65°N) where nitrate is supplied to the Arctic Ocean [*Le Fouest et al*., 2013; *Torres-Valdés et al*., 2013] and decreases interiorward as nitrate is removed from surface waters by biological processes and inflowing waters subduct below the halocline [*Hioki et al*., 2014]. The simulation broadly captures observed nitrate concentrations along the transect, with the exception of the Chukchi shelf where simulated upstream concentrations advected in from the Pacific are too high and observational biases toward summer may also bias the comparison [*Brown et al*., 2015]. We note that few observations are available for the Central Basin.

3.3. Predicting the Vertical Distribution of Production

A composite of observational time series suggests a consistent seasonal cycle of vertical production distributions across the Arctic Ocean. Supply of nitrate to the euphotic zone across the Arctic Ocean is dominated by entrainment in the winter mixed layer [*Sundfjord et al*., 2007, 2008; *Tremblay and Gagnon*, 2009; *Codispoti et al*., 2013; *Randelhoff et al*., 2015]. Because temperatures are cold and exhibit relatively small vertical variability across the Arctic Ocean [*Steele et al*., 2001], vertical changes in phytoplankton nitrate uptake rates during the following growing season are determined by light. Therefore, seasonal nitracline deepening rates across the Arctic Ocean may depend on the surface nitrate inventory at the time of maximum mixed-layer depths and solar radiation dose the following summer.

Phytoplankton respond to nitracline deepening by more growth in the water column occurring at depth [*Martin et al*., 2010; *McLaughlin and Carmack*, 2010; *Bergeron and Tremblay*, 2014]. Therefore, the vertical distribution of production over an annual cycle may be determined by the winter-entrained nitrate inventory and summer solar radiation dose. Spatial maps of simulated subsurface production fraction, nitrate

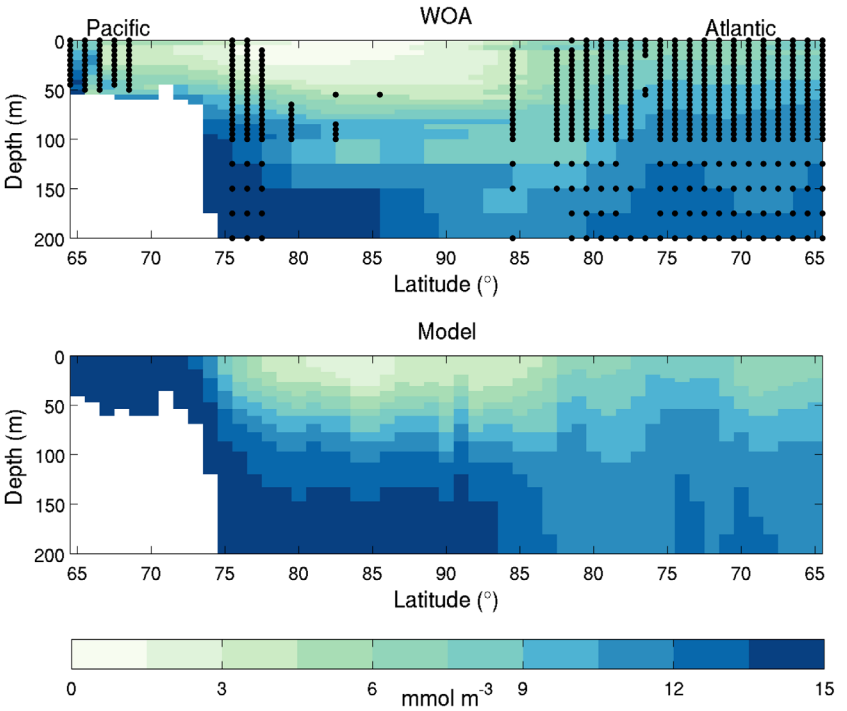

Figure 2. Transect of annual mean (top) observed (World Ocean Atlas) and (bottom) simulated Arctic dissolved inorganic nitrogen in the surface ocean (mmol m^{-3}). The transect runs from Bering Straits to Fram Straits (65°N–90°N at 169°W and 5°W), as shown in Figure 3a. Grid squares containing observations are shown by black dots in the top of the figure (number of observations = 5923). Observation distribution is biased toward lower latitudes (toward 65°N).

inventory, and solar radiation dose demonstrate this (Figure 3). The subsurface fraction of production is higher where the nitrate inventory is lower or solar radiation dose is higher: such as in the Beaufort Gyre and Admunsen Gulf, where stratification and Ekman convergence prevent entrainment of nitrate into surface waters [*Martin et al*., 2010; *McLaughlin and Carmack*, 2010] and our simulation (Figure 3c) and observations [*Tremblay et al*., 2008; *Mundy et al*., 2009; *Martin et al*., 2010] concur that a substantial proportion of annual production happens in subsurface chlorophyll maxima. Conversely, in low light areas, subsurface production is low (Figure 3).

A simple multilinear regression model based on colocated N_{inv} and SRD captures 73% of the simulated variance in the subsurface fraction of annual production (Figure 4). Therefore, the contribution phytoplankton growth at depth makes to depth-integrated annual production is predictable from colocated N_{inv} and SRD.

To examine the spatial variability of simulated vertical production distributions, we split the Arctic Ocean into three geographic regions (Figure 4, inset). First, we delineate inflows as waters exterior of main gateways and the Central Arctic Ocean as interior waters. A third region is then used to show the transformation of water masses as they transit across the Canadian Arctic Ocean from the Pacific inflow to their outflow along the west side of Baffin Bay [*Curry et al*., 2014].

Examining the vertical distribution of production across these three regions then shows the relationship between this subsurface fraction, ice cover, and physical nitrate supply. Around the edge of the Arctic Ocean, ice-free (high SRD, Figure 3b) conditions enable substantial production at depth (Figure 4). Conversely, in the Central Basin and the Chukchi inflow, extensive ice cover (low SRD, Figure 3b) prevents substantial production at depth (Figure 4). SRD and the subsurface fraction increase toward the inflows where ice cover is reduced (Figure 3).

As water masses transit from the Pacific inflow across the Canadian Arctic Ocean, they experience nitrate depletion due to phytoplankton uptake [*Tremblay et al*., 2008] and denitrification [*Yamamoto-Kawai et al*., 2006; *Chang and Devol*, 2009]. Subduction of nitrate replete waters [*Hioki et al*., 2014] and Ekman convergence in the Beaufort Gyre [*McLaughlin and Carmack*, 2010] further reduces N_{inv}.

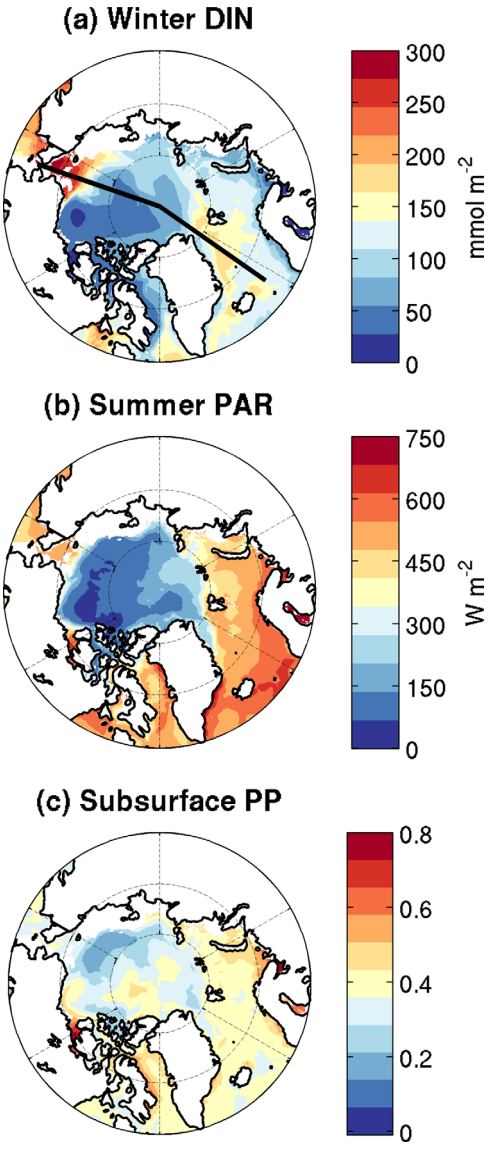

Figure 3. Decade-mean (2000s) simulated (a) winter (month of colocated max mixed layer depth) dissolved inorganic nitrogen (DIN) inventory (N_{inv}, mmol m^{-2}), (b) summer-mean (July–September) solar photosynthetically active irradiance (PAR) dose (SRD, Wm^{-2}), (c) proportion of annual primary production that occurs below 20 m (Subsurface PP). Water depths <50 m are masked in all plots to prevent bias of the subsurface fraction in Figure 3c. The location of the transect plotted in Figure 2 is shown in Figure 3a (black line).

Depletion of N_{inv} in our simulation drives deepening of production maxima, resulting in an increasing subsurface fraction of production as waters move across the Canadian Arctic Ocean (Figure 4). The broad pattern that arises is modulated by ice cover such that the light replete Admunsen Gulf has the highest proportion of production subsurface (Figure 3).

Our simulation demonstrates that reduced N_{inv} causes deepening of production distributions. A higher proportion of annual growth then occurs at depth (>0.5) where light-dependent growth rates are lower. However, under thicker ice, SRD is too low to support net photosynthesis at depth so the subsurface fraction is low (<0.3) despite low N_{inv} (Figure 3).

In the first case, depth-integrated production rates are reduced because surface nitrate depletion necessitates phytoplankton grow at depth where light is lower. In the second case, rates are lower because ice cover reduces light over the entire water column. Therefore, depth-integrated production decreases toward low and high subsurface fractions of production, being maximum at intermediate subsurface fractions. In our simulation, intermediate subsurface fractions correspond to inflows, in agreement with observational-based estimates of depth-integrated production which are also maximum here [*Sakshaug*, 2004; *Arrigo et al*., 2008; *Pabi et al*., 2008; *Codispoti et al*., 2013; *Hill et al*., 2013].

This analysis suggests that CMIP5 21st-century projections of N_{inv} reductions and SRD increases, that are robust across the ensemble [*Vancoppenolle et al*., 2013], may cause deepening of production distributions. The impact of increased light over the water column on depth-integrated production would then be offset by reduced light experienced by deeper growth. We now demonstrate this response in the full simulation.

3.4. Phytoplankton Response to an Ice-Free Arctic

The Arctic Ocean is predicted to be ice free by the end of the century [*Boé et al*., 2009], and perhaps as early as 2054–2058 [*Liu et al*., 2013]. Physical nitrate supply to surface waters is expected to decrease as Arctic sea ice retreats and light increases [*Vancoppenolle et al*., 2013].

Here we simulate the onset of a seasonally ice-free Arctic Ocean in the 2050s and a modest reduction in mixed-layer depth from the present day to 2099 (Figure 5a). Unrealistic fluctuations in simulated winter mixed layer depth arise from localized overmixing in the model south of Fram Strait and do not impact Arctic-average N_{inv} (Figure 5b).

Reducing surface nitrate (Figure 5b) induces the expansion of low surface nitrate waters (Figure 6a). Deepening of the nitracline and increased light induces deepening of geographically colocated chlorophyll and production maxima (Figures 5c and 6c) as phytoplankton adjust to the perturbed nitrate and light conditions. Phytoplankton

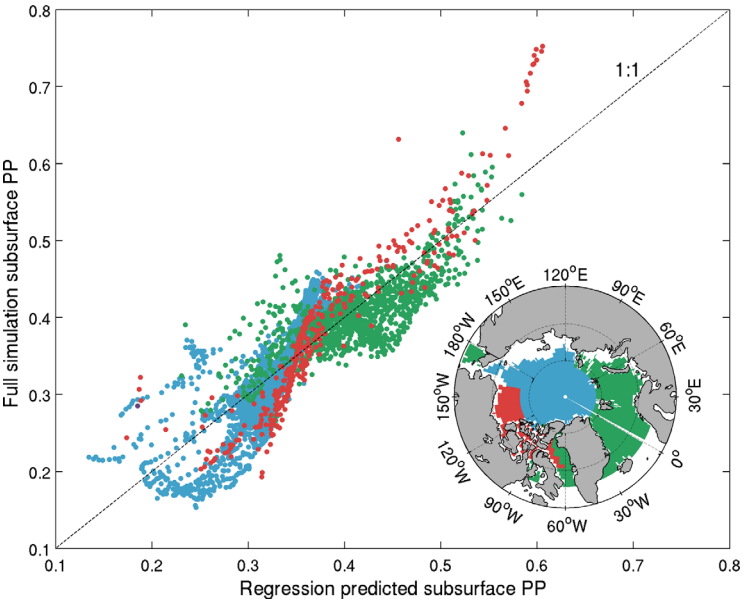

Figure 4. The simulated (2000s) proportion of annual production occurring subsurface (below 20 m) plotted against that predicted by a linear regression model based on N_{inv} and SRD. First, we construct the linear regression model which regresses N_{inv} and SRD to Prop (PropReg = 0.000430 SRD − 0.00120 N_{inv} + 0.355, $R^2 = 0.731$, $p < 0.001$). Data are grouped into three geographical regions: inflows, central Arctic, and the Canadian Arctic, as shown on the inset map. Baffin Bay is split between the Canadian Arctic Outflow to the west and West Greenland Current influenced waters to the east. Water depths <50 m are masked (as in Figure 3) to prevent bias of the subsurface production fraction.

maxima deepen more slowly than the nitracline, resulting in increasingly offset depths which reflect the increase in light limitation with depth. This is in agreement with the observed phytoplankton response to low light at depth in oligotrophic conditions [*McLaughlin and Carmack*, 2010; *Bergeron and Tremblay*, 2014]. Reductions in N_{inv} occur in both Pacific and Atlantic inflows but extremely low inventories (<50 mmol m^2) are only reached in the Atlantic inflow because the decreasing trend starts from a lower present-day inventory here. N_{inv} decreases in both inflows in the simulation because nitrate supply that originates in the subpolar North Atlantic and Pacific decreases in the coming century, in agreement with most CMIP5 models [*Vancoppenolle et al.*, 2013].

Simulated depth-integrated production changes reflect the ability of SRD increases to compensate reduced N_{inv} (Figure 6d). We broadly simulate decreasing production in open water and increasing production within the present ice zone, in agreement with ensemble projections [*Steinacher et al.*, 2010; *Vancoppenolle et al.*, 2013]. This broad pattern is modulated by regional differences in nitrate supply. N_{inv} reductions fully offset SRD increases in the Beaufort Gyre and exceed them downstream where present-day ice cover is thinner and less extensive. Reduced advective nitrate supply to the Siberian shelves exceeds modest SRD increases here.

As the ice retreats and N_{inv} diminishes, SRD increases over the water column are offset by reduced light experienced by deeper phytoplankton growth. Simulated production increases in a future Arctic Ocean are therefore modest. They are 10% at the onset of a seasonally ice-free Arctic Ocean and 30% by the end of the century, with increases occurring solely at depth (Figure 5d).

Phytoplankton metabolic rates are temperature dependent, therefore future Arctic Ocean production changes may be sensitive to ocean warming [*Slagstad et al.*, 2011]. We test the direct impact of sea surface temperature increases on production by using the temperature dependence of simulated phytoplankton growth rates (equation (2)).

We find that despite substantial warming of water flowing into the Arctic Ocean (6–8°C, Figure 7a), direct temperature effects on phytoplankton growth are more modest (40–60%, Figure 7b) compared to SRD and N_{inv} effects across the Arctic Ocean (up to 220%, Figure 6d). Substantial direct temperature-driven increases are restricted to inflows because warmer inflowing surface waters are cooled as they are advected into the Arctic Ocean. Inflowing surface waters where warming occurs generally retain surplus nitrate (Figure 6b) indicating that most of the direct simulated temperature impacts correspond to realized production changes.

4. Discussion

We have shown that vertical production distributions across the Arctic Ocean are governed by local balances in N_{inv} and SRD. N_{inv}-SRD balances that result in low or high subsurface fractions of production lead to

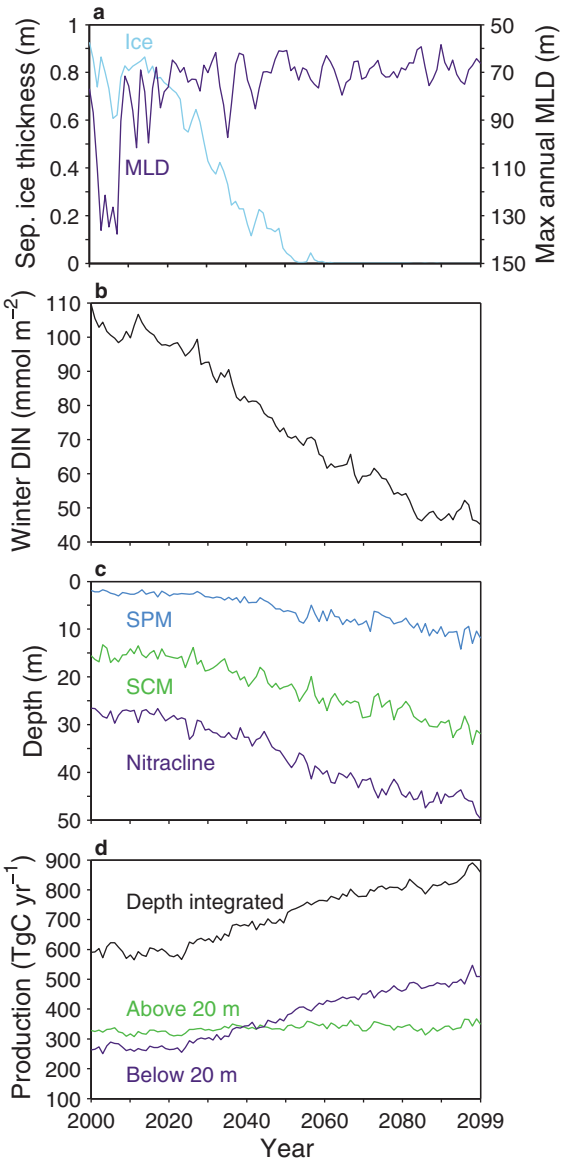

Figure 5. Arctic-average (>65°N) simulated 21st century trends in (a) September ice thickness (ice) and maximum annual mixed layer depth (MLD, m), (b) winter dissolved inorganic nitrogen (DIN) inventory (N_{inv}, mmol m^{-2}), (c) September production maxima (SPM), chlorophyll maxima (SCM), and nitracline depths (m), and (d) annual surface, subsurface and total production (Tg C yr^{-1}).

low depth-integrated annual production. We have demonstrated that nitrate reductions act to deepen production distributions where light-dependent growth rates are lower, provided light at depth is sufficient to support net growth (Figures 3 and 4). Therefore, CMIP5 projections of reducing N_{inv} [*Vancoppenolle et al.*, 2013] are expected to deepen future production distributions such that increases in SRD due to ice retreat are offset by lower light levels experienced at greater depth (Figures 5 and 6).

In the simulation, low N_{inv} waters are found over the Beaufort Gyre (Figure 6b). Simple process models suggest that sea ice decline will increase Beaufort Gyre convergence [*Davis et al.*, 2014]. Recent convergence has reduced N_{inv} [*McLaughlin and Carmack*, 2010], suggesting that increased convergence under ice retreat may play a role in future N_{inv} reductions in the Beaufort Sea and downstream Canadian Archipelago. Our simulation shows such a change, with some of the largest relative reductions in production arising from convergence in the Beaufort Sea and downstream low N_{inv} waters (Figure 6d).

Large Arctic Ocean production decreases are colocated with September production maxima deepening, except on the Siberian shelves where water depths are too shallow (Figures 6c and 6d). Maxima deepening does not occur across the Arctic Ocean but is localized to extremely low N_{inv} waters. The explanation for this can be found in our analysis of contemporary forcing of phytoplankton distributions by surface nitrate conditions. We have shown that surface nitrate depletion acts to deepen production distributions but may only do so when there is sufficient light to enable production at depth. Therefore, our analysis predicts deepening of production distributions across a broad area of the future Arctic Ocean, verified in the simulation where production increases (Figure 6d) are taken up at depth (Figure 5d). However, production maxima correspond to the depth of minimal nitrate-light colimitation. Since light attenuates exponentially with depth, light limitation increases rapidly with depth and extremely low nitrate concentrations are required to deepen production maxima. For this reason, simulated production maxima deepening is colocated with extremely low surface nitrate concentrations (Figures 6b and 6c).

In elucidating the controls on vertical production distributions, we assumed temperature effects on growth rates are small because vertical temperature gradients in the Arctic Ocean are small. We subsequently demonstrated that this assumption is valid by predicting vertical production distributions with a regression model that neglects temperature (Figure 4). Further, projected depth-integrated production changes are dependent on increases in sea surface temperature (SST) which directly affect growth rates. The contribution of direct temperature effects is shown to be more modest than SRD-N_{inv}-driven changes at the pan-

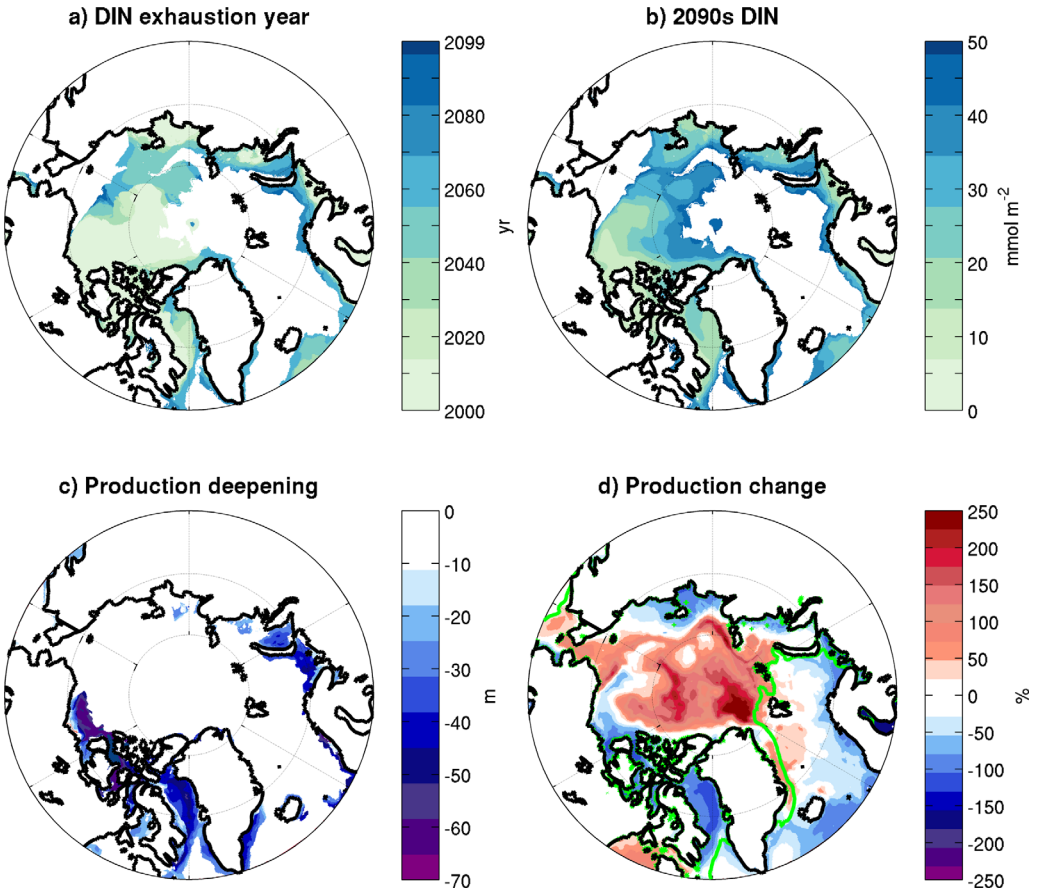

Figure 6. Twenty-first century changes in simulated dissolved inorganic nitrogen and primary production. (a) Onset year at which N_{inv} first drops below 50 mmol m^{-2} (masked areas do not reach this threshold). (b) The 2090s N_{inv} (mmol m^{-2}), masked to only show locations where the inventory is below 50 mmol m^{-2}. (c) The 2090s to 2000s change in September production maxima depth (m) (negative values indicate deepening). (d) The 2090s to 2000s change in annual production (%) with 2000s winter-average (January–March) 95% ice cover contour (green line).

Arctic Ocean scale, failing to compensate N_{inv}-driven reductions in inflows (Figures 6 and 7). We stress that direct temperature effects, as defined here (equation (2)), can only impact production in light and nitrate replete conditions. Therefore, one reason for more modest contributions from direct temperature effects

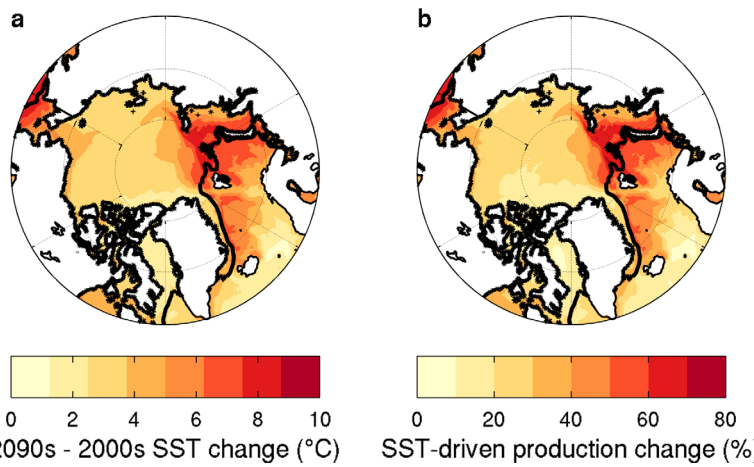

Figure 7. Simulated 2090s to 2000s change in (a) sea surface temperature (SST, °C) and (b) direct temperature-driven production increases (%). The simulated present-day (2000s) winter-average (January–March) 95% ice cover contour is shown (black line).

could be that N_{inv} reductions negate the possibility of SST-driven annual production increases being realized because growth rates may be temperature dependent but annually integrated production increases require available nitrate. In the simulation, SST-driven increases generally occur outside areas where severely limiting nitrate concentrations are projected (Figures 6b and 7b), implying that SST-driven production increases are realized here and are locally important in offsetting N_{inv} reductions in inflows. SST effects on production generally do not overlap with low N_{inv} waters because nitrate is supplied to the surface Arctic Ocean in warm, nitrate replete inflows [*Torres-Valdés et al*., 2013], which are cooled and depleted of nitrate as they move interiorward into the Arctic Ocean.

We have shown the impact of N_{inv} and SRD on the vertical distribution of production by using a reference depth of 20 m. Now that we have elucidated the impacts of N_{inv} and SRD on the vertical distribution of growth, we can explain what the significance of our choice is. Light limitation increases with depth and nitrate limitation decreases with depth. It is the opposing effects of these limitations that promote deepening of production distributions following exhaustion of surface nitrate in summer (Figures 3 and 4) and enables production maxima to be subsurface in extremely low nitrate conditions (Figure 6). We chose a reference depth based on observed vertical distributions of phytoplankton to highlight these opposing limitations, 20 m being the approximate depth at which the limitations balance.

Therefore, the analysis presented here is not sensitive per se to the reference depth, but at extreme reference depths one of nitrate or light limitation dominates and we end up with the trivial results that occur at the limits. For example, if we chose a very deep reference depth and define SRD and N_{inv} as being integrated from the surface to the reference depth then light limitation will dominate at all locations in the Arctic Ocean. Conversely, if we chose a very shallow reference depth then nitrate limitation dominates. Further, with shallow reference depths Prop (equation (1)) tends toward 1 and with deep reference depths toward 0. Therefore, with deep reference depths, we arrive at the result that light limitation dominates nitrate limitation so growth is restricted to above the reference depth. At shallow reference depths, nitrate limitation dominates so growth is predominantly below the reference depth.

From this, it can be seen that while all reference depths produce consistent and physically sound results, choosing the right reference depth is necessary to see the full impact of nitrate and light limitation on the vertical distribution of Arctic Ocean production.

Models within the CMIP5 ensemble agree on a reduction in N_{inv} contemporary with ice retreat yet disagree on the sign of future production changes [*Vancoppenolle et al*., 2013]. Our analysis replicates the N_{inv} trend (Figure 5b) and suggests why the current ensemble production projections diverge. Divergence may arise because the model hindcasts generally inadequately reproduce both N_{inv} and SRD [*Vancoppenolle et al*., 2013], shown here to be central features of Arctic Ocean production dynamics and its anthropogenic perturbation. In particular, models differ in the extent of vertical mixing and most fail to account for production under ice [*Vancoppenolle et al*., 2013], likely substantial across the ice-covered Arctic Ocean [*Arrigo et al*., 2012; *Matrai and Apollonio*, 2013; *Arrigo et al*., 2014]. Differences between models in the magnitude of nitrate reduction trend compound model divergence [*Vancoppenolle et al*., 2013] but an essential prerequisite to evaluating this divergence will be hindcasts that adequately represent the processes elucidated here.

5. Conclusions

We have used a simulation of Arctic Ocean phytoplankton that reproduces observed chlorophyll and nitrate distributions to show that phytoplankton respond to colocated N_{inv} reductions and SRD increases by deepening of colocated production distributions. The spatial pattern of vertical production distributions (Figure 4) can therefore be related to local nitrate and light conditions (Figure 3).

Because N_{inv} reductions and SRD increases deepen production distributions, CMIP5 ensemble projections of reduced N_{inv} concomitant with ice retreat can be inferred to deepen future production distributions (Figures 5c and 6c). Therefore, light increases due to ice retreat are offset by lower light experienced by deeper production distributions.

Resulting Arctic Ocean production increases are modest, 10% in a seasonally ice-free Arctic, increasing to 30% by the end of the century, and occur at depth (Figure 5d).

Acknowledgments
We gratefully acknowledge the Forum for Arctic Modeling and Observational Synthesis (FAMOS, http://web.whoi.edu/famos/) for providing a forum for stimulating discussion which informed this manuscript. Observational data used in the analysis are available as cited in the manuscript. Model simulation results and code used in the analysis are available on request. The authors gratefully acknowledge the financial support of the Natural Environmental Research Council (NERC). The simulation work was performed as part of the Regional Ocean Modelling project (ROAM; grant NE/H017372/1), part of the NERC UK Ocean Acidification research programme (UKOA). J.L. is funded by a NERC PhD studentship. E.E.P., M.A.S., and A.Y. are supported by NERC National Capability funding. The high-resolution component of this work used the ARCHER UK National Supercomputing Service (http://www.archer.ac.uk). The HadGEM2-ES atmospheric forcing was produced by the UKMO and made available for use in NEMO by Dan Bernie (UKMO). Work to perform HadGEM2-ES simulations was supported by the EU-FP7 COMBINE project (grant 226520).

References

Ardyna, M., M. Babin, M. Gosselin, E. Devred, L. Rainville, and J.-É. Tremblay (2014), Recent Arctic Ocean sea ice loss triggers novel fall phytoplankton blooms, *Geophys. Res. Lett.*, *41*, 6207–6212, doi:10.1002/2014GL061047.

Arrigo, K., G. van Dijken, and S. Pabi (2008), Impact of a shrinking Arctic ice cover on marine primary production, *Geophys. Res. Lett.*, *35*, L19603, doi:10.1029/2008GL035028.

Arrigo, K., P. Matrai, and G. van Dijken (2011), Primary productivity in the Arctic Ocean: Impacts of complex optical properties and subsurface chlorophyll maxima on large-scale estimates, *J. Geophys. Res.*, *116*, C11022, doi:10.1029/2011JC007273.

Arrigo, K., et al. (2012), Massive phytoplankton blooms under Arctic sea ice, *Science*, *336*(6087), 1408–1408, doi:10.1126/science.1215065.

Arrigo, K., et al. (2014), Phytoplankton blooms beneath the sea ice in the Chukchi Sea, *Deep Sea Res., Part II*, *105*, 1–16, doi:10.1016/j.dsr2.2014.03.018.

Arrigo, K. R., and G. L. van Dijken (2015), Continued increases in Arctic Ocean primary production, *Prog. Oceanogr.*, *136*, 60–70, doi:10.1016/j.pocean.2015.05.002.

Bergeron, M., and J.-É. Tremblay (2014), Shifts in biological productivity inferred from nutrient drawdown in the southern Beaufort Sea (2003–2011) and northern Baffin Bay (1997–2011), Canadian Arctic, *Geophys. Res. Lett.*, *41*, 3979–3987, doi:10.1002/2014GL059649.

Bintanja, R., and F. Selten (2014), Future increases in Arctic precipitation linked to local evaporation and sea-ice retreat, *Nature*, *509*(7501), 479–482, doi:10.1038/nature13259.

Boé, J., A. Hall, and X. Qu (2009), September sea-ice cover in the Arctic Ocean projected to vanish by 2100, *Nat. Geosci.*, *2*(5), 341–343, doi:10.1038/ngeo467.

Brown, Z., K. Lowry, M. A. Palmer, G. van Dijken, M. Mills, R. Pickart, and K. Arrigo (2015), Characterizing the subsurface chlorophyll a maximum in the Chukchi Sea and Canada Basin, *Deep Sea Res., Part II*, *118*, 88–104, doi:10.1016/j.dsr2.2015.02.010.

Carmack, E., and D. C. Chapman (2003), Wind-driven shelf/basin exchange on an Arctic shelf: The joint roles of ice cover extent and shelf-break bathymetry, *Geophys. Res. Lett.*, *30*(14), 1778, doi:10.1029/2003GL017526.

Chang, B. X., and A. H. Devol (2009), Seasonal and spatial patterns of sedimentary denitrification rates in the Chukchi Sea, *Deep Sea Res., Part II*, *56*(17), 1339–1350, doi:10.1016/j.dsr2.2008.10.024.

Codispoti, L., V. Kelly, A. Thessen, P. Matrai, S. Suttles, V. Hill, M. Steele, and B. Light (2013), Synthesis of primary production in the Arctic Ocean: III. Nitrate and phosphate based estimates of net community production, *Prog. Oceanogr.*, *110*, 126–150, doi:10.1016/j.pocean.2012.11.006.

Collins, W., et al. (2011), Development and evaluation of an Earth-System model–HADGEM2, *Geosci. Model Dev.*, *4*(4), 1051–1075, doi:10.5194/gmdd-4-997-2011.

Curry, B., C. Lee, B. Petrie, R. Moritz, and R. Kwok (2014), Multiyear volume, liquid freshwater, and sea ice transports through Davis Strait, 2004–10, *J. Phys. Oceanogr.*, *44*(4), 1244–1266, doi:10.1175/JPO-D-13-0177.1.

Davis, P. E., C. Lique, and H. L. Johnson (2014), On the link between Arctic sea ice decline and the freshwater content of the Beaufort Gyre: Insights from a simple process model, *J. Clim.*, *27*(21), 8170–8184, doi:10.1175/JCLI-D-14-00090.1.

Eppley, R. W. (1972), Temperature and phytoplankton growth in the sea, *Fish. Bull*, *70*(4), 1063–1085.

Garcia, H., R. Locarnini, T. Boyer, J. Antonov, O. Baranova, M. Zweng, J. Reagan, and D. Johnson (2014), *World Ocean Atlas 2013, vol. 4, Dissolved Inorganic Nutrients (Phosphate, Nitrate, Silicate)*, A. Mishonov Technical ed., pp. 1–25, US Govern. Print. Off., Washington, D. C.

Giles, K. A., S. W. Laxon, A. L. Ridout, D. J. Wingham, and S. Bacon (2012), Western Arctic Ocean freshwater storage increased by wind-driven spin-up of the Beaufort Gyre, *Nat. Geosci.*, *5*(3), 194–197, doi:10.1038/ngeo1379.

Hill, V., and G. Cota (2005), Spatial patterns of primary production on the shelf, slope and basin of the Western Arctic in 2002, *Deep Sea Res., Part II*, *52*(24), 3344–3354, doi:10.1016/j.dsr2.2005.10.001.

Hill, V., P. Matrai, E. Olson, S. Suttles, M. Steele, L. Codispoti, and R. Zimmerman (2013), Synthesis of integrated primary production in the Arctic Ocean: II. In situ and remotely sensed estimates, *Prog. Oceanogr.*, *110*, 107–125, doi:10.1016/j.pocean.2012.11.005.

Hioki, N., et al. (2014), Laterally spreading iron, humic-like dissolved organic matter and nutrients in cold, dense subsurface water of the Arctic Ocean, *Sci. Rep.*, *4*, 6775, doi:10.1038/srep06775.

Laxon, S. W., et al. (2013), Cryosat-2 estimates of Arctic sea ice thickness and volume, *Geophys. Res. Lett.*, *40*, 732–737, doi:10.1002/grl.50193.

Le Fouest, V., M. Babin, and J.-É. Tremblay (2013), The fate of riverine nutrients on Arctic shelves, *Biogeosci. Discuss.*, *10*(6), 3661–3677, doi:10.5194/bg-10-3661-2013.

Li, W. K., F. A. McLaughlin, C. Lovejoy, and E. C. Carmack (2009), Smallest algae thrive as the Arctic Ocean freshens, *Science*, *326*(5952), 539–539, doi:10.1126/science.1179798.

Liu, J., M. Song, R. M. Horton, and Y. Hu (2013), Reducing spread in climate model projections of a September ice-free Arctic, *Proc. Natl. Acad. Sci. U. S. A.*, *110*(31), 12,571–12,576, doi:10.1073/pnas.1219716110.

Madec, G. (2008), *NEMO Ocean Engine*, Inst. Pierre-Simon Laplace, Paris, France.

Martin, J., J.-É. Tremblay, J. Gagnon, G. Tremblay, A. Lapoussière, C. Jose, M. Poulin, M. Gosselin, Y. Gratton, and C. Michel (2010), Prevalence, structure and properties of subsurface chlorophyll maxima in Canadian Arctic waters, *Mar. Ecol. Prog. Ser.*, *412*, 69–84, doi:10.3354/meps08666.

Martin, J., D. Dumont, and J. Tremblay (2013), Contribution of subsurface chlorophyll maxima to primary production in the Coastal Beaufort Sea (Canadian Arctic): A model assessment, *J. Geophys. Res. Oceans*, *118*, 5873–5886, doi:10.1002/2013JC008843.

Matrai, P., and S. Apollonio (2013), New estimates of microalgae production based upon nitrate reductions under sea ice in Canadian shelf seas and the Canada Basin of the Arctic Ocean, *Mar. Biol.*, *160*(6), 1297–1309, doi:10.1007/s00227-013-2181-0.

Matrai, P., E. Olson, S. Suttles, V. Hill, L. Codispoti, B. Light, and M. Steele (2013), Synthesis of primary production in the Arctic Ocean: I. Surface waters, 1954-2007, *Prog. Oceanogr.*, *110*, 93–106, doi:10.1016/j.pocean.2012.11.004.

McLaughlin, F. A., and E. C. Carmack (2010), Deepening of the nutricline and chlorophyll maximum in the Canada Basin interior, 2003–2009, *Geophys. Res. Lett.*, *37*, L24602, doi:10.1029/2010GL045459.

McLaughlin, F. A., E. C. Carmack, A. Proshutinsky, R. A. Krishfield, C. K. Guay, M. Yamamoto-Kawai, J. M. Jackson, and W. J. Williams (2011), The rapid response of the Canada Basin to climate forcing: From bellwether to alarm bells, *Oceanography*, *24*(3), 146–159.

Monod, J. (1949), The growth of bacterial cultures, *Annu. Rev. Microbiol.*, *3*, 371–394.

Mundy, C., M. Gosselin, J. Ehn, Y. Gratton, A. Rossnagel, D. Barber, J. Martin, J.-É. Tremblay, M. Palmer, and K. Arrigo (2009), Contribution of under-ice primary production to an ice-edge upwelling phytoplankton bloom in the Canadian Beaufort Sea, *Geophys. Res. Lett.*, *36*, L17601, doi:10.1029/2009GL038837.

Pabi, S., G. van Dijken, and K. Arrigo (2008), Primary production in the Arctic Ocean, 1998–2006, *J. Geophys. Res.*, *113*, C08005, doi:10.1029/2007JC004578.

Peterson, B. J., J. McClelland, R. Curry, R. M. Holmes, J. E. Walsh, and K. Aagaard (2006), Trajectory shifts in the Arctic and SubArctic freshwater cycle, *Science*, *313*(5790), 1061–1066, doi:10.1126/science.1122593.

Popova, E., A. Coward, G. Nurser, B. De Cuevas, M. Fasham, and T. Anderson (2006), Mechanisms controlling primary and new production in a global ecosystem model? Part I: Validation of the biological simulation, *Ocean Sci.*, *2*(2), 249–266.

Popova, E., A. Yool, A. Coward, Y. Aksenov, S. Alderson, B. D. Cuevas, and T. Anderson (2010), Control of primary production in the Arctic by nutrients and light: Insights from a high resolution ocean general circulation model, *Biogeosci. Discuss.*, *7*(4), 5557–5620, doi:10.5194/bg-7-3569-2010.

Popova, E., A. Yool, A. Coward, F. Dupont, C. Deal, S. Elliott, E. Hunke, M. Jin, M. Steele, and J. Zhang (2012), What controls primary production in the Arctic Ocean? Results from an intercomparison of five general circulation models with biogeochemistry, *J. Geophys. Res.*, *117*, C00D12, doi:10.1029/2011JC007112.

Proshutinsky, A., R. Bourke, and F. McLaughlin (2002), The role of the Beaufort Gyre in Arctic climate variability: Seasonal to decadal climate scales, *Geophys. Res. Lett.*, *29*(23), 2100, doi:10.1029/2002GL015847.

Rainville, L., and R. A. Woodgate (2009), Observations of internal wave generation in the seasonally ice-free Arctic, *Geophys. Res. Lett.*, *36*, L23604, doi:10.1029/2009GL041291.

Randelhoff, A., A. Sundfjord, and M. Reigstad (2015), Seasonal variability and fluxes of nitrate in the surface waters over the Arctic shelf slope, *Geophys. Res. Lett.*, *42*, 3442–3449, doi:10.1002/2015GL063655.

Riahi, K., S. Rao, V. Krey, C. Cho, V. Chirkov, G. Fischer, G. Kindermann, N. Nakicenovic, and P. Rafaj (2011), RCP 8.5: A scenario of comparatively high greenhouse gas emissions, *Clim. Change*, *109*(1–2), 33–57, doi:10.1007/s10584-011-0149-y.

Sakshaug, E. (2004), Primary and secondary production in the Arctic Seas, in *The Organic Carbon Cycle in the Arctic Ocean*, pp. 57–81, Springer, London, U. K.

Serreze, M. C., M. M. Holland, and J. Stroeve (2007), Perspectives on the Arctic's shrinking sea-ice cover, *Science*, *315*(5818), 1533–1536, doi:10.1126/science.1139426.

Slagstad, D., I. Ellingsen, and P. Wassmann (2011), Evaluating primary and secondary production in an Arctic Ocean void of summer sea ice: an experimental simulation approach, *Prog. Oceanogr.*, *90*(1), 117–131, doi:10.1016/j.pocean.2011.02.009.

Smith, R. (1980), Remote-sensing and depth distribution of ocean chlorophyll, *Mar. Ecol. Prog. Ser.*, *5*, 359–361.

Steele, M., R. Morley, and W. Ermold (2001), PHC: A global ocean hydrography with a high-quality Arctic Ocean, *J. Clim.*, *14*(9), 2079–2087.

Steinacher, M., et al. (2010), Projected 21st century decrease in marine productivity: A multi-model analysis, *Biogeosciences*, *7*(3), 979–1005, doi:10.5194/bg-7-979-2010.

Stroeve, J. C., M. C. Serreze, M. M. Holland, J. E. Kay, J. Malanik, and A. P. Barrett (2012), The Arctic's rapidly shrinking sea ice cover: A research synthesis, *Clim. Change*, *110*(3-4), 1005–1027, doi:10.1007/s10584-011-0101-1.

Sundfjord, A., I. Fer, Y. Kasajima, and H. Svendsen (2007), Observations of turbulent mixing and hydrography in the marginal ice zone of the Barents Sea, *J. Geophys. Res.*, *112*, C05008, doi:10.1029/2006JC003524.

Sundfjord, A., I. Ellingsen, D. Slagstad, and H. Svendsen (2008), Vertical mixing in the marginal ice zone of the northern Barents Sea–Results from numerical model experiments, *Deep Sea Res., Part II*, *55*(20), 2154–2168, doi:10.1016/j.dsr2.2008.05.027.

Timmermann, R., H. Goosse, G. Madec, T. Fichefet, C. Ethe, and V. Duliere (2005), On the representation of high latitude processes in the ORCA-LIM global coupled sea ice–ocean model, *Ocean Modell.*, *8*(1), 175–201, doi:10.1016/j.ocemod.2003.12.009.

Torres-Valdés, S., T. Tsubouchi, S. Bacon, A. C. Naveira-Garabato, R. Sanders, F. A. McLaughlin, B. Petrie, G. Kattner, K. Azetsu-Scott, and T. E. Whitledge (2013), Export of nutrients from the Arctic Ocean, *J. Geophys. Res. Oceans*, *118*, 1625–1644, doi:10.1002/jgrc.20063.

Tremblay, J.-É., and J. Gagnon (2009), The effects of irradiance and nutrient supply on the productivity of Arctic waters: A perspective on climate change, in *Influence of Climate Change on the Changing Arctic and Sub-Arctic Conditions*, pp. 73–93, Springer, London, U. K.

Tremblay, J.-É., K. Simpson, J. Martin, L. Miller, Y. Gratton, D. Barber, and N. M. Price (2008), Vertical stability and the annual dynamics of nutrients and chlorophyll fluorescence in the Coastal, Southeast Beaufort Sea, *J. Geophys. Res.*, *113*, C07S90, doi:10.1029/2007JC004547.

Vancoppenolle, M., L. Bopp, G. Madec, J. Dunne, T. Ilyina, P. R. Halloran, and N. Steiner (2013), Future Arctic Ocean primary productivity from CMIP5 simulations: Uncertain outcome, but consistent mechanisms, *Global Biogeochem. Cycles*, *27*(3), 605–619, doi:10.1002/gbc.20055.

Yamamoto-Kawai, M., E. Carmack, and F. McLaughlin (2006), Nitrogen balance and Arctic throughflow, *Nature*, *443*(7107), 43, doi:10.1038/443043a.

Yool, A., E. Popova, and T. Anderson (2013), Medusa-2.0: An intermediate complexity biogeochemical model of the marine carbon cycle for climate change and ocean acidification studies, *Geosci. Model Dev.*, *6*, 1767–1811, doi:10.5194/gmd-6-1767-2013.